Eur. Phys. J. A **23**, 365–378 (2005)
DOI 10.1140/epja/i2004-10085-9

THE EUROPEAN PHYSICAL JOURNAL A

Neutrino scattering rates in the presence of hyperons from a Skyrme model in the RPA approximation

L. Mornas[a]

Departamento de Física, Universidad de Oviedo, Avda Calvo Sotelo 18, 33007 Oviedo, Spain

Received: 9 August 2004 /
Published online: 16 December 2004 –
Communicated by V. Vento

Abstract. The contribution of Λ-hyperons to neutrino scattering rates is calculated in the random phase approximation in a model where the interaction is described by a Skyrme potential. Finite temperature and neutrino trapping are taken into account in view of applications to the deleptonization stage of protoneutron star cooling. The hyperons can remove the problem of ferromagnetic instability common to (nearly) all Skyrme parametrizations of the nucleon-nucleon interaction. As a consequence, there is not any longer a pole at the transition in the neutrino-baryon cross-section. However there still remains an enhancement in this region. In the absence of ferromagnetism the mean free path in $np\Lambda$ matter is reduced compared to its value in np matter as a consequence of the presence of this additional degree of freedom. At high density the results are very sensitive to the choice of the Λ-Λ interaction.

PACS. 26.60.+c Nuclear matter aspects of neutron stars – 25.30.Pt Neutrino scattering – 21.60.Jz Hartree-Fock and random-phase approximations

1 Introduction

During and shortly after the collapse of a supernova, a copious amount of neutrinos is produced. The hope that these neutrinos could permit a successful explosion in numerical simulations through the Wilson (delayed) mechanism, together with the increase of available computational power, has triggered an important effort in designing a new generation of computer codes. The Boltzmann equation for neutrino transport can now be solved simultaneously with the equations for the hydrodynamical evolution of the supernova explosion (see, *e.g.*, [1]). The differential cross-section for the various neutrino production, absorption and scattering processes is a key input in the Boltzmann equation. These calculations also yield the spectral characteristics of the corresponding neutrino burst, which are now well within the reach of modern detectors. Although the current picture is that neutrinos alone are not enough to prevent shock stall, but 3-D fluid flow with convection is also necessary, the solution of the Boltzmann equation still seems to be an unavoidable requirement of a supernova explosion simulation. It is therefore necessary to have as good as possible a description of the neutrino interaction with matter and of the influence of medium effects, chemical composition and temperature on this data.

[a] e-mail: lysiane@pinon.ccu.uniovi.es

The neutrino-nucleon cross-section and the influence of nuclear correlations on this parameter in the central protoneutron star have been estimated by several authors both in relativistic and nonrelativistic models [2–13]. While it is generally found in relativistic models that medium effects tend to reduce the scattering rate, the findings from nonrelativistic models are less clear cut. The nonrelativistic calculations on the other hand have been performed with a greater variety of assumptions as to the nature of nuclear correlations taken into consideration as the relativistic ones.

A key issue is whether a ferromagnetic instability is excited at high density. In this case it would appear as a pole in the neutrino-nucleon cross-section when the nuclear correlations are calculated in the random phase approximation [10,11]. Such a feature is commonly observed when the nuclear interaction is described by a Skyrme force. It has been traced to the exchange (Fock) term. A ferromagnetic transition is actually also possible in relativistic models [14,15] treated in the Hartree-Fock approximation. A relativistic calculation of neutrino-nucleon scattering at the RPA level and including exchange terms however has yet to be performed. Then again in nonrelativistic models the susceptibility has been found to increase and a ferromagnetic state to be energetically unfavourable in recent calculations where the nuclear interaction is extracted from Brueckner-Hartree-Fock calculations [12,13].

At later times hyperons begin to appear and affect the luminosities as well as the equation of state [16]. One can hope to detect the tail of this neutrino burst (between 20 and 50 seconds after the beginning of the signal), which corresponds to the cooling of the still hot but partially deleptonized protoneutron star. In these later stages the diffusion equation is thought to be a good approximation, the neutrino dynamics then enter in the mean free path. After ~ 50 s, the neutron star has cooled to temperatures of the order of 1 MeV and achieved full deleptonization, *i.e.* the neutrinos are no longer trapped. It then enters in a long cooling phase. The mean free path is no longer the relevant parameter; instead, the available cooling codes need as an input the neutrino emissivity.

The aim of this work is to assess the relevance of the hyperonic degree of freedom on the neutrino interaction with neutron star matter with a simple description of the interactions, before appealing to the heavier machinery of microscopical description through the Brueckner-Hartree-Fock calculations or taking into account the relativistic effects. We have chosen for this purpose the Skyrme interaction parametrized by Lanskoy *el al.* [17–19]. This description includes the Λ-hyperons with parameters fitted with the available data on hypernuclei. It is also able to give a description of neutron stars in agreement with the results of more refined models [20].

Our model is described in sect. 2 with a presentation of the chosen Skyrme parametrizations in sects. 2.1-2.3 and of the necessary formalism for the calculation of the cross-section in sect. 2.4. Section 2.5 discusses the influence of hyperons on a possible ferromagnetic instability and sect. 3 gives an estimate of the evolution of the hyperon fraction during the deleptonization of the protoneutron star. We then present results for the vector and axial response functions and differential cross-section in sect. 4.1 and for the mean free path in protoneutron star matter in sect. 4.2. Section 5 summarizes the main results and gives a brief discussion of how the model could be improved.

2 Formalism

2.1 Skyrme forces

Besides the usual parameterization of the nucleon-nucleon interaction

$$\begin{aligned} V_{NN}(r_1-r_2) &= t_0\,(1+x_0P_\sigma)\delta(r_1-r_2) \\ &+\frac{1}{2}t_1\,(1+x_1P_\sigma)\left[k'^2\;\delta(r_1-r_2)+\delta(r_1-r_2)\;k^2\right] \\ &+t_2\,(1+x_2P_\sigma)k'\,\delta(r_1-r_2)\,k \\ &+\frac{1}{6}t_3\,(1+x_3P_\sigma)\,\rho_N^\alpha\left(\frac{r_1+r_2}{2}\right)\delta(r_1-r_2), \end{aligned} \tag{1}$$

we use the following Lambda-nucleon and Lambda-Lambda potentials as suggested, *e.g.*, by Lanskoy *et al.* [17,18]:

$$\begin{aligned} V_{N\Lambda}(r_N-r_\Lambda) &= u_0\,(1+y_0P_\sigma)\delta(r_N-r_\Lambda) \\ &+\frac{1}{2}u_1\,\left[k'^2\;\delta(r_N-r_\Lambda)+\delta(r_N-r_\Lambda)\;k^2\right] \\ &+u_2\,k'\,\delta(r_N-r_\Lambda)\,k \\ &+\frac{3}{8}u_3\,(1+y_3P_\sigma)\rho_N^\beta\left(\frac{r_N+r_\Lambda}{2}\right)\delta(r_N-r_\Lambda)\,, \end{aligned} \tag{2}$$

$$\begin{aligned} V_{\Lambda\Lambda}(r_1-r_2) &= \lambda_0\delta(r_1-r_2) \\ &+\frac{1}{2}\lambda_1\left[k'^2\;\delta(r_1-r_2)+\delta(r_1-r_2)\;k^2\right] \\ &+\lambda_2\,k'\,\delta(r_1-r_2)\,k+\lambda_3\,\rho_\Lambda\rho_N^\gamma\,. \end{aligned} \tag{3}$$

(We haved dropped in these expressions the spin-orbit terms which will not be used in the remainder of this paper.)

While this model only includes the Λ-hyperon, and would seem less complete than, *e.g.*, the model of Balberg and Gal [21] which includes all the hyperons, we fixed our choice on the former because these authors provide the two-particle potential. This permitted us to derive the Landau parameters for the spin-1 as well as for the spin-0 channels. The Landau parameters in the spin-1 channel are namely necessary for the calculation of the axial structure function in the RPA approximation. By contrast, Balberg and Gal [21] give directly a parametrization of the (unpolarized) energy density functional. This parametrization can therefore only be used in the mean-field approximation. While thermodynamical relationships can give access to the Landau parameters in the spin-0 channel, we have no way of determining those of the spin-1 channel. Since the axial structure function is known to give the dominant contribution to the neutrino cross-section, this precludes the use of the model of Balberg in the RPA approximation. We will nevertheless use the model of Balberg and Gal at the mean-field level in order to estimate the error committed by neglecting other hyperons and in particular the Σ^-.

Some *a posteriori* justification may be given for a model with the Λ-hyperon only: i) The parametrization of the $N\Lambda$ and $\Lambda\Lambda$ is relatively well grounded on Brueckner-Hartree-Fock calculations and duly cross-checked with data on single and double Λ-hypernuclei. By contrast, experimental data concerning the Σ-hyperon is quite scarce. ii) It is argued from recent analysis of Σ^- atoms and the absence of a clear signal for the formation of bound Σ states in (K^-,π) reactions [22–24], as well as from calculations in quark models [25,26], that the Σ single-particle potential is probably repulsive in nuclear matter. β-equilibrium calculations performed on the basis of this assumption predict that the threshold for Σ-hyperon formation in neutron stars is shifted to very large densities. If such be the case, they would concern only a minor fraction of the star or even not appear at all (see, *e.g.*, [21,27]). iii) We are still concerned here with investigating qualitative effects, namely the influence of a new degree of freedom on the scattering rate and the effect of hyperon formation on preventing an eventual ferromagnetic transition.

Table 1. Skyrme parameters for the NN interaction [28–30].

Model	α	t_0	t_1	t_2	t_3	x_0	x_1	x_2	x_3
SLy10	1/6	2506.77	430.98	−304.95	13826.41	1.0398	−0.6745	−1.0	1.6833
SkI3	1/4	−1762.88	561.608	−227.09	8106.2	0.3083	−1.1722	−1.0907	1.2926
SV	1	−1248.3	970.6	107.2	0.	−0.17	0.	0.	1.

Table 2. Skyrme parameters for the $N\Lambda$ and $\Lambda\Lambda$ interactions [17–19].

Model	β	u_0	u_1	u_2	u_3	y_0	y_3
LY-I	1/3	−476.	42.	23.	1514.1	−0.0452	−0.280
YBZ-6	1	−372.2	100.4	79.60	2000.	−0.107	0.

Model	λ_0	λ_1
SLL2	−437.7	240.
no LL	0	0

2.2 Composition of matter in chemical equilibrium

In neutron star matter we impose that the conditions for β equilibrium are fulfilled. We write the equality of the chemical potentials $\hat{\mu} = (\mu_n + m_n) - (\mu_p + m_p) = \mu_e - \mu_\nu$, $\mu_n + m_n = \mu_\Lambda + m_\Lambda$. We must also impose electric charge conservation $n_e = n_p$. At a given baryonic density the electron, proton and hyperon fractions are determined by the solution of these three equations. The chemical potentials are determined by deriving the Skyrme energy density functional with respect to the density of the corresponding particle. Their explicit expression was given in a companion paper [20]. The electrons are relativistic and their chemical potential is given by $\mu_e = \sqrt{k_{Fe}^2 + m_e^2}$. In protoneutron star matter with trapped neutrinos we have $\mu_\nu = (6\pi^2 n_\nu)^{(2/3)}$, while in colder neutrino-free neutron star matter $\mu_\nu = 0$. The muons were not considered for simplicity, as their presence is not expected to lead to qualitative changes in the results. The threshold density for Λ-hyperon formation is determined by the condition $\mu_\Lambda(\mathrm{thr}) = \mu_\Lambda(k_{F\Lambda} = 0) = \mu_n + m_n - m_\Lambda$. The hyperons form around 2-3 n_{sat} in neutrino-free matter, they appear at higher density when neutrinos are trapped in the star.

2.3 Skyrme parametrizations of the hyperonic sector

In [20] we have examined many combinations of parameters for the Skyrme forces among those available in the literature in the light of their suitability for the description of neutron star physics (tables 1 and 2). We settled on a recent parametrization by Reinhard and Flocard [28] in the nucleon sector SkI3 (or the very similar SkI5) together with the set YBZ6 for the nucleon-Λ interaction among those recommended by Lanskoy *et al.* [17,19] as offering one of the best description of hypernuclear data. For the Λ-Λ interaction we then considered two options, either the SLL2 force of Lanskoy [18] or no interaction. Lanskoy fitted the binding excess to $\Delta B_{\Lambda\Lambda} = -4.8$ MeV, *i.e.* more atttractive than the presently accepted value of −1 MeV. The truth should hopefully lie between these two choices.

All expected properties for the neutron star structure were then recovered. Very importantly, the ferromagnetic transition common to (nearly) all Skyrme models is avoided when hyperons are present (see sect. 2.5).

Table 3. Thresholds for hyperon formation and for ferromagnetism in $np\Lambda e$ matter in β equilibrium.

Model	$n_{\mathrm{thr}}^{\Lambda}$	Y_p	n_{ferro}
SLy10+LY-I+SLL2	2.719	0.041	6.183
SkI3+YBZ6+SLL2	2.076	0.144	9.194
SV+YBZ6+SLL2	1.951	0.136	9.093

Among the main results obtained with the SkI3+YBZ6+SLL2 parametrization, let us mention:

– The equation of state is softened by the presence of the hyperon degrees of freeedom. As a consequence, the maximum mass (2.26 $M_\odot$) for a npe star is reduced to 1.64 $M_\odot$ for a star with hyperons.

– A hot star with trapped neutrinos was observed to be metastable in the mass range [1.64–1.88] $M_\odot$, as noticed in several earlier studies, see, *e.g.*, [31]. A protoneutron star in this mass range will eventually collapse to a black hole as it undergoes deleptonization.

– The equation of state remains causal in the whole star when hyperons are present.

– The Λ-hyperons appear at a threshold density 2.08 n_{sat} in cold neutrino-free matter. In protoneutron star matter with a lepton fraction $Y_L = 0.4$, the formation of hyperons is delayed until 2.85 n_{sat}.

– The asymmetry energy $a_A = (1/2)\partial(E/A)/\partial\beta^2|_{\beta\to 0}$ increases rapidly with density with the SkI3 parametrization, allowing for high proton fractions.

– There exists a non-negligible hyperon fraction in the core of the protoneutron star before deleptonization is fully completed (see sect. 3). The tail of the supernova neutrino burst which corresponds to this stage could therefore be affected by the presence of hyperons.

Another suitable set was the Skyrme Lyon SLy10 [29] together with the LYI parametrization of the N-Λ force also favored by Lanskoy. The asymmetry energy increases with density but much slower than with the SkI3 force; as a consequence, the proton fraction remains rather low. With hyperons the maximum mass of the neutron star was a lower but still acceptable 1.425 $M_\odot$. The set SLy10 was preferred over the more widely used SLy4 and SLy7 sets because it was easier to keep it clear of the ferromagnetic

Table 4. Conditions for causality and neutron star properties.

Model	$n_B(c_s^2=1)$	$n_c(1.4\ M_\odot)$	$R(1.4\ M_\odot)$	$n_{\max}$	$M_{\max}$	$R(M_{\max})$
SLy10, *npe* matter	7.308	3.60	11.05	7.69	1.99	9.52
SLy10+LY-I+SLL2	16.032	9.38	9.0	12.38	1.425	8.11
SkI3, *npe* matter	6.343	2.27	13.21	6.12	2.263	11.16
SkI3+YBZ6, no LL	causal	2.36	13.20	4.66	1.655	12.52
SkI3+YBZ6+SLL2	13.077	2.39	13.19	6.79	1.642	11.02
SV, *npe* matter	4.983	2.10	13.46	5.44	2.426	11.54
SV+YBZ6, no LL	causal	2.19	13.40	4.44	1.662	12.75
SV+YBZ6+SLL2	13.082	2.22	13.41	6.5	1.639	11.24

pole. In other respects the properties of SLy10 are very similar to that of the Sly4 and Sly7 sets.

Finally we singled out the older SV force [30]. This set is rather atypical as it has $t_3 = 0$, its effective mass at saturation is also lower ($m_* = 0.38$) than the commonly accepted values. Although its adequacy for reproducing the properties of nuclei and nuclear matter is somewhat less satisfactory than was the case for SkI3 or SLy10, it has the unique feature of not presenting a ferromagnetic transition in nuclear matter nor in *npe* matter in β equilibrium which makes it very valuable for comparison purposes. Its general characteristics (stiffness and maximum neutron star mass, proton content) are quite similar to those of the SkI3 set.

We reproduce in tables 3 and 4 the relevant entries of the tables published in [20].

2.4 Neutrino-baryon scattering and absorption rates

In the nonrelativistic approximation the differential scattering cross-section for the process $\nu(p_1) + B(p_2) \rightarrow \nu(p_3) + B(p_4)$ is taken to be (see, *e.g.*, [2,5,10,11]):

$$\frac{1}{V}\frac{\mathrm{d}\sigma}{\mathrm{d}\omega \mathrm{d}\Omega} = \frac{G_F^2}{8\pi^3}(E'_\nu)^2[1-f(E'_\nu)] \times \Big[(1+\cos\theta)\mathcal{S}^{(0)}(\omega,k) + (3-\cos\theta)\mathcal{S}^{(1)}(\omega,k)\Big]. \quad (4)$$

In this expression, ω and k are the transferred energy and momentum $p_1^\mu - p_3^\mu = (\omega, \vec{k})$, $E'_\nu = E_\nu - \omega$ is the neutrino energy after the collision and θ is the scattering angle $\vec{p}_1.\vec{p}_3 = |p_1|\,|p_3|\,\cos\theta$. The structure functions $\mathcal{S}^{(S)}$ in spin channel S are defined by the expectation value of the density and spin density fluctuations in baryonic matter. In the mean-field approximation they both reduce to

$$\mathcal{S}_0 = 2\int \frac{\mathrm{d}^3 p_2}{(2\pi)^3}\frac{\mathrm{d}^3 p_4}{(2\pi)^3} f(p_2)(2\pi)^4 \times \delta^4(p_1+p_2-p_3-p_4)\,(1-f(p_4))\,. \quad (5)$$

They are related to the imaginary part of the reducible polarizations by

$$\mathcal{S}^{(S)}(\omega,k) = -2\frac{1}{1-e^{-\beta(\omega+\tilde{\mu})}}\ \mathcal{I}\mathrm{m}\,\Pi^{(S)}(\omega,k)\,. \quad (6)$$

This definition differs by a factor $1/\pi$ from that of [10,11, 32] but agrees with that of [4,5] so that the elastic limit be $\mathcal{S}_0(\omega,k) \rightarrow 2\pi n_B \delta(\omega)$

In the nonrelativistic limit, the spin-0 and spin-1 responses correspond to the vector and axial couplings, respectively. In the random phase approximation the vector and axial structure functions obey uncoupled Dyson equations:

$$\Pi^{\mathrm{RPA}}_{V/A} = \Pi_0 + \Pi^{\mathrm{RPA}}_{V/A}\ V_{(S=0/1)}\ \Pi_0, \quad (7)$$

where

$$\Pi_0 = \frac{2}{(2\pi)^3}\int \mathrm{d}^3 p\ \left[\frac{f(E_p)-f(E_{p+q})}{q_0+E_p-E_{p+q}+i\epsilon}\right] \quad (8)$$

and $V_{(S=0/1)}$ the interaction potential in the particle-hole channel.

In our case, the Dyson equation has a 3×3 matrix structure. The RPA polarization is obtained by inverting (7) with

$$\Pi_0 = \begin{bmatrix} \Pi_n^0 & 0 & 0 \\ 0 & \Pi_p^0 & 0 \\ 0 & 0 & \Pi_\Lambda^0 \end{bmatrix}. \quad (9)$$

We have for the real part of the polarizations

$$\mathcal{R}\mathrm{e}\ \Pi_0^i(\omega,k) = \frac{m_i^*}{2\pi^2 k}\int_0^\infty p\mathrm{d}p \ln\left[\frac{(k^2-2kp)^2-(2m_i^*\omega)^2}{(k^2+2kp)^2-(2m_i^*\omega)^2}\right]\ f(E_i), \quad (10)$$

with $f(E_i) = \left\{1+\exp\left[\left(\frac{p^2}{2m_i^*}-\tilde{\mu}_i\right)/T\right]+1\right\}^{-1}$ and $\tilde{\mu}_i = \mu_i - \mathcal{U}_i$.

The expressions for the effective masses and chemical potential were given in the appendix of [20]. At $T = 0$, $\mathcal{R}\mathrm{e}\ \Pi_0^i$ reduces to the Linhardt function in agreement with, *e.g.*, [32]:

$$\mathcal{R}\mathrm{e}\ \Pi_0^i(\omega,k) \stackrel{T\rightarrow 0}{\longrightarrow} -\frac{m_i^* p_{Fi}}{2\pi^2}\ [1+\phi_i(x_+)+\phi_i(x_-)]\,, \quad (11)$$

$$\phi_i(x) = \frac{p_{Fi}}{2k}\ [1-x]\ \ln\left|\frac{1+x}{1-x}\right|\,,$$

$$x_\pm = \frac{k}{2p_{Fi}} \pm \frac{\omega m_i^*}{k p_{Fi}}\,.$$

The imaginary part is always analytical

$$\mathcal{I}\mathrm{m}\ \Pi_0^i(\omega,k) = -\frac{(m_i^*)^2 T}{2\pi k} \times \ln\left\{\frac{1+\exp\left[-\left(\frac{p_-^2}{2m_i^*}-\tilde{\mu}_i\right)/T\right]}{1+\exp\left[-\left(\frac{p_+^2}{2m_i^*}-\tilde{\mu}_i\right)/T\right]}\right\}, \quad \text{with} \quad p_\pm = p_{Fi}x_\pm\,. \tag{12}$$

We will extract the potential in the Landau Fermi Liquid approximation from the Skyrme parameterization. Our potential has no imaginary part in this approximation. We will be working in the simplest monopolar ($l=0$) Landau approximation; our potential has therefore no angular or momentum dependence. For a discussion of the full RPA with momentum dependence we refer the reader to [10,11,33,34].

The potential in the vector isovector channel for neutrino scattering through the neutral current process is given in our model in terms of the Landau parameters f_{ij}

$$V_{(S=0)} = \begin{bmatrix} f_{nn} & f_{np} & f_{n\Lambda} \\ f_{pn} & f_{pp} & f_{p\Lambda} \\ f_{\Lambda n} & f_{\Lambda p} & f_{\Lambda\Lambda} \end{bmatrix}. \tag{13}$$

For the axial channel, one should replace all f_{ij} by the g_{ij} in order to obtain the relevant potential $V_{(S=1)}$. The Landau parameters can be extracted from the Skyrme potential energy by applying a double functional differentiation with respect to occupation numbers [32,33]. Their explicit expression when hyperons are present was given in [20].

After performing the inversion, we obtain for example in the axial ($S=1$) channel

$$\Pi_{A\,nn}^{\mathrm{RPA}} = \frac{1}{\mathrm{Det}[I - V_{(S=1)}\,\Pi_0]} \times \left[(1-g_{pp}\Pi_p^0)(1-g_{\Lambda\Lambda}\Pi_\Lambda^0) - g_{p\Lambda}^2\Pi_p^0\Pi_\Lambda^0\right]\Pi_n^0, \tag{14}$$

$$\Pi_{A\,np}^{\mathrm{RPA}} = \frac{1}{\mathrm{Det}[I - V_{(S=1)}\,\Pi_0]} \times \left[(1-g_{\Lambda\Lambda}\Pi_\Lambda^0)g_{pn} + g_{p\Lambda}g_{n\Lambda}\Pi_\Lambda^0\right]\Pi_p^0\Pi_n^0\,, \tag{15}$$

$$\Pi_{A\,n\Lambda}^{\mathrm{RPA}} = \frac{1}{\mathrm{Det}[I - V_{(S=1)}\,\Pi_0]} \times \left[(1-g_{pp}\Pi_p^0)g_{n\Lambda} + g_{np}g_{p\Lambda}\Pi_n^0\right]\Pi_n^0\Pi_\Lambda^0\,, \tag{16}$$

with similar expressions for the vector channel ($S=0$). These equations reduce to eqs. (26)-(32) of Reddy *et al.* [7] when no hyperons are present.

Let us note at this stage that if the determinant appearing in the denominator is strongly reduced or vanishes, this will give rise to a corresponding peak in the structure function and in the neutrino cross-section. This is indeed what happens in the axial channel for previous calculations [10,11] in pure neutron matter and *npe* matter in β equilibrium (see also fig. 16 of [7]): The condition

$$D_A = \mathrm{Det}[I - V_{(S=1)}\,\Pi_0] = 0 \tag{17}$$

is fulfilled at some critical density, signalling the transition to a ferromagnetic state. This is discussed further in next section.

Finally the structure functions appearing in eq. (4) are obtained from

$$S_{V/A} = \begin{pmatrix} c_{V/A}^p & c_{V/A}^n & c_{V/A}^\Lambda \end{pmatrix} \cdot \begin{pmatrix} S_{V/A}^{pp} & S_{V/A}^{pn} & S_{V/A}^{p\Lambda} \\ S_{V/A}^{np} & S_{V/A}^{nn} & S_{V/A}^{n\Lambda} \\ S_{V/A}^{\Lambda p} & S_{V/A}^{\Lambda n} & S_{V/A}^{\Lambda\Lambda} \end{pmatrix} \cdot \begin{pmatrix} c_{V/A}^p \\ c_{V/A}^n \\ c_{V/A}^\Lambda \end{pmatrix}, \tag{18}$$

with

$$c_V^p = \frac{1}{2}(1-4\sin^2\theta_W) = 0.04\,, \quad c_V^n = -\frac{1}{2}\,, \quad c_V^\Lambda = -\frac{1}{2}\,;$$
$$c_A^p = \frac{1}{2}(D+F) = \frac{1.26}{2}\,, \quad c_A^n = -\frac{1}{2}(D+F) = -\frac{1.26}{2}\,,$$
$$c_A^\Lambda = -\frac{1}{2}(F+D/3) = -0.365\,. \tag{19}$$

2.5 Poles in the dispersion relations

Previous studies on the neutrino mean free path in neutron matter [10] or npe^- matter in β equilibrium [11] found that a pole appears in the calculation of the axial structure function above a certain critical density. This feature is typical of Skyrme parameterization of nuclear interactions and is related to a transition to a ferromagnetic state.

In [20] we defined the magnetic susceptibilities χ_{ij}, where $i,j \in \{n,p,\Lambda\}$. The inverse susceptibilities are proportional to the second derivatives of the energy density functional with respect to the polarizations:

$$\frac{\mu_i\mu_j}{\chi_{ij}} = \frac{2\rho}{\rho_i\rho_j}\Delta_{ij}\,, \tag{20}$$

$$\Delta_{ij} = \frac{1}{2}\frac{\partial^2(\mathcal{E}/\rho)}{\partial s_i \partial s_j}\,, \tag{21}$$

$$s_i = \frac{\rho_{i\uparrow} - \rho_{i\downarrow}}{\rho_{i\uparrow} + \rho_{i\downarrow}}\,. \tag{22}$$

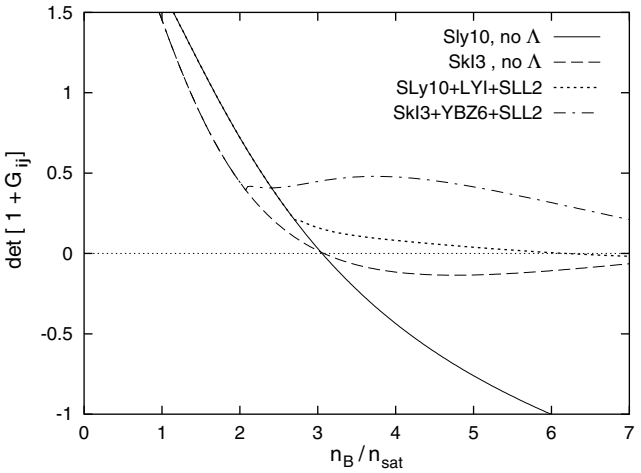

Fig. 1. Criterion for the transition to a ferromagnetic state.

t (s)	0	5	10	15	20	25	30	35	40	45	50
T (MeV)	17.3	25.0	31.7	36.5	37.5	36.5	33.6	29.8	26.0	22.1	18.3
Y_L	0.345	0.315	0.283	0.256	0.239	0.222	0.202	0.178	0.145	0.119	0.09

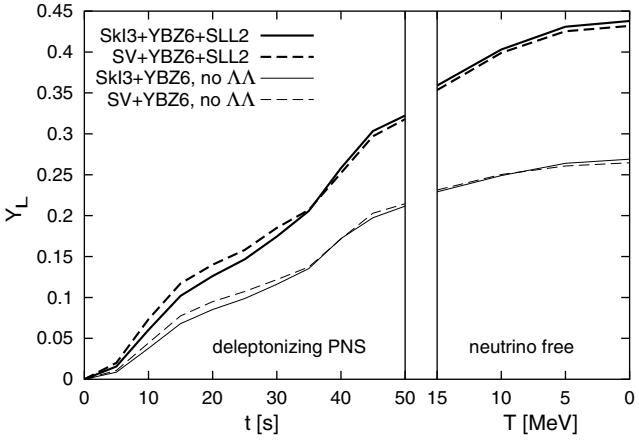

Fig. 2. Evolution of the hyperonic content as a function of time.

On the other hand it can be shown that the Δ_{ij} are related to the Landau parameters g_0^{ij} through

$$\Delta_{ij} = \frac{2\rho}{\rho_i \rho_j} \frac{1}{\sqrt{N_0^i N_0^j}} G_0^{ij}\,, \quad \text{if } i \neq j\,,$$
$$\Delta_{ii} = \frac{2\rho}{\rho_i^2} \frac{1}{N_0^i}(1 + G_0^{ii})\,,$$
$$G_0^{ij} = \sqrt{N_0^i N_0^j}\, g_0^{ij}\,, \qquad N_0^i = \frac{m_i^* k_{Fi}}{\pi^2 \hbar^2}\,. \tag{23}$$

A criterion for the appearance of the ferromagnetic phase is that the determinant of the inverse susceptibility matrix vanishes, or equivalently, in terms of the Landau parameters:

$$\mathrm{Det} \begin{pmatrix} (1+G_0^{nn}) & G_0^{np} & G_0^{n\Lambda} \\ G_0^{pn} & (1+G_0^{pp}) & G_0^{p\Lambda} \\ G_0^{\Lambda n} & G_0^{p\Lambda} & (1+G_0^{\Lambda\Lambda}) \end{pmatrix} = 0\,. \tag{24}$$

In the limit where the temperature T and the energy transfer ω go to zero, the real part of the Linhardt functions tend to the limiting value

$$\mathcal{R}\mathrm{e}\, \Pi_0^i(\omega, k) \overset{(T\to 0,\, \omega\to 0,\, \omega/k=\mathrm{cst})}{\longrightarrow} -N_0^i\,. \tag{25}$$

If we further assume that the imaginary part of the polarizations vanish (which, even though it turns out to be an excellent approximation, is not strictly the case) we would then find that the condition that a pole appears in the dressed axial polarization $\mathrm{Det}[I - V_{(S=1)}\Pi_0]$ (cf. eq. (17)) is identical to the criterion for the appearance of a ferromagnetic phase defined in this section. In fact the finite imaginary parts provide for some Landau damping of the pole. The pole will also be somewhat shifted and smoothed by finite temperature, but this hardly changes our conclusions in practice for the temperatures relevant for protoneutron stars (up to 30 MeV).

In [20] we plotted the criterion (24) as a function of density. It was shown that when the threshold for hyperon formation was lower than the critical density for the ferromagnetic transition in *npe* matter, the hyperons were able to stabilize the system so that the pole could be avoided. An example of these results is displayed in fig. 1.

A similar study can be performed for the vector response function. The denominator $D_V = \mathrm{Det}[I - V_{(S=0)}\,\Pi_0] = 0$ reduces at $T = 0$, $\omega \to 0$ to the criterion for instability under density fluctuations equivalent to eq. (24) by replacing the G_{ij} by the corresponding F_{ij}. At low density, no hyperons are present, and the criterion reduces to that for spinodal instability in asymmetric nuclear matter (see, *e.g.*, [35]) $(1+F_0^{nn})(1+F_0^{pp}) - (F_0^{np})^2 = 0$. The pole disappears at temperatures $\sim$ 15 MeV, but the enhancement persists at higher temperatures.

3 Evolution of the hyperonic content in a deleptonizing protoneutron star

As the protoneutron star cools and the trapped neutrinos are released, the beta equilibrium becomes more favorable to the production of hyperons. If a sizable number of hyperons appear before the deleptonization is completed, the mean free path of the neutrinos will be affected and could influence the characteristics of the tail of the neutrino burst detected in supernova explosions. The determination of the evolution of the hyperonic content would require to solve self-consistently the equations for thermodynamical conditions, neutrino mean free path, diffusion of neutrinos and cooling along the lines of reference [16].

In this section we take the results from fig. 17 of Pons *et al.* [16] as representative of the evolution of the temperature and leptonic content. With this input we calculate the structure of the neutron star at each time step. While this procedure is not consistent, it still permits to estimate whether hyperons will be relevant at this stage.

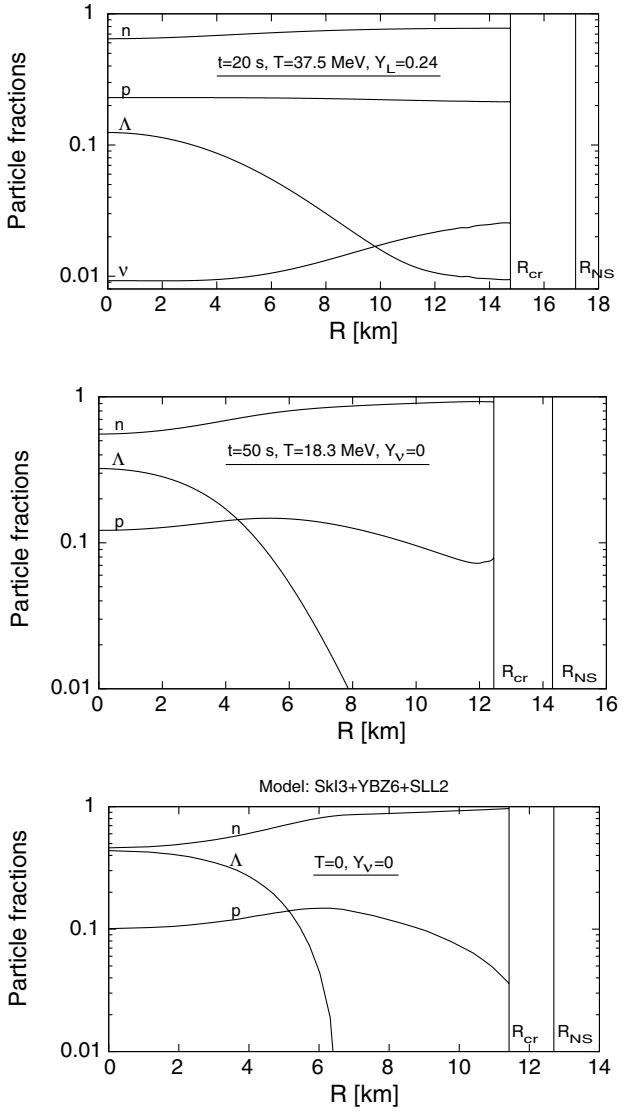

Fig. 3. Particle fractions as a function of the neutron star radius at three stages of the deleptonization.

We chose the evolution curves correponding to model GM3 with hyperons (curved labeled GM3npH in [16]). The temperature T and total lepton number $Y_L = Y_e + Y_\nu$ are fixed to values extracted from fig. 17 of [16] (see table above fig. 2). The central density was also taken according to the results of [16] but was rescaled for each parameter set in order to match with a 1.6 $M_\odot$ neutron star at the end of deleptonization. It was checked that the equation of state and chemical composition at the end of deleptonization obtained by setting $Y_L = 0.09$ coincides with that obtained when setting $Y_\nu = 0$.

After neutrinos have left the neutron star, it continues to cool from $T = 18.3$ MeV to $T = 0$. We perfomed four more calculations at $T = 0$, 5, 10 and 15 MeV to follow the hyperonic content in this later stage. The result is displayed in figs. 2 and 3 for the parameter sets which allow a stable neutron star with a mass 1.6 $M_\odot$, namely SkI3 or SV in the nucleon sector, YBZ6 for the hyperon-nucleon interaction and either no Lambda-Lambda interaction or the SLL2 parametrization of Lanskoy *et al.*

In fig. 2 the hyperonic fraction at the center of the star is displayed as a function of time. We can see that a sizable fraction of hyperons is present as early as 10 seconds after the collapse. The result are very similar whether we use the SkI3 or SV force. On the other hand we again note a strong dependence on the characteristics of the Λ-Λ interaction.

Figure 3 shows the density profile of the neutron star at three stages of the deleptonization ($t = 20$ s, $t = 50$ s and $t \to \infty$) for the parameter set SkI3+YBZ6+SLL2. As the star cools, its radius shrinks and the hyperons gather at its center.

4 Neutrino scattering rates

4.1 Structure functions

a) Axial response

Let us first discuss the behaviour of the contributions to the axial structure functions from neutrons ($S_A^{(nn)}$), protons ($S_A^{(pp)}$) and Λ hyperons ($S_A^{(\Lambda\Lambda)}$).

As already obtained by other authors [10,11], the axial structure function for neutrons in *npe* matter displays a strong enhancement at $\omega = 0$, going over to a pole at the critical density $n_{\rm ferro}^{\beta\text{-}npe}$. We have seen in sect. 2.5, the criterion for ferromagnetic instability is equal to the condition that the denominator of the dressed polarizations vanish at $\omega = 0$. This is a mechanical instability, meaning that an infinitesimal energy fluctuation $\omega = \varepsilon$ can trigger the phase transition. This should not be confused with the phenomenon of spin zero sound analogous to the zero sound mode observed in the vector response function, where a peak appears at a finite value $\omega = \omega_{ZS}$. In the latter case the response function displays a resonance corresponding to the excitation of a collective motion of the system at the corresponding velocity v_{ZS}.

Figure 4 compares the axial structure functions obtained in the mean-field and random phase approximations. The system is *npeΛ* matter in β equilibrium at a density $n_B = 4\ n_{\rm sat}$, temperature $T = 10$ MeV and we fixed the transferred momentum at $k = 30$ MeV. The interactions are described by the choice of parameters SkI3 + YBZ6 + SLL2. While the RPA correction is only moderate in the $S_A^{(pp)}$ and $S_A^{(\Lambda\Lambda)}$ contributions, we can clearly see the enhancement due to the vicinity of the ferromagnetic criterion in $S_A^{(nn)}$. On the other hand, no spin zero sound peak is observed at a finite value of ω.

Figure 5 compares the $S_A^{(nn)}$ as a function of density for three different Skyrme parametrizations: SLy10+LYI+SLL2, SkI3+YBZ6+SLL2 and SV+YBZ6+SLL2. At saturation the three parametrizations give very similar results. At three time saturation density on the other hand the quantity $D_A(\omega = 0) = \mathrm{Det}(1 + G_{ij})$ is approaching the zero axis for the SkI3 and SLy10 models (see fig. 1) and the $S_A^{(nn)}$

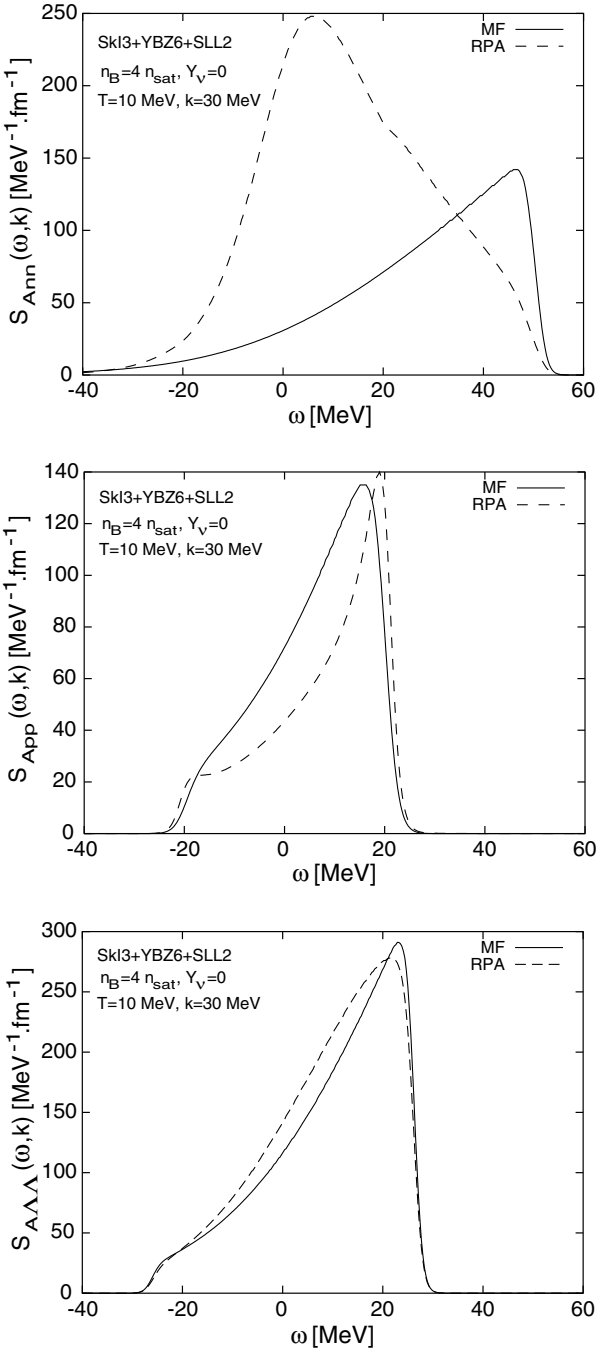

Fig. 4. Axial structure functions in $npe\Lambda$ matter in beta equilibrium —mean-field and RPA approximations.

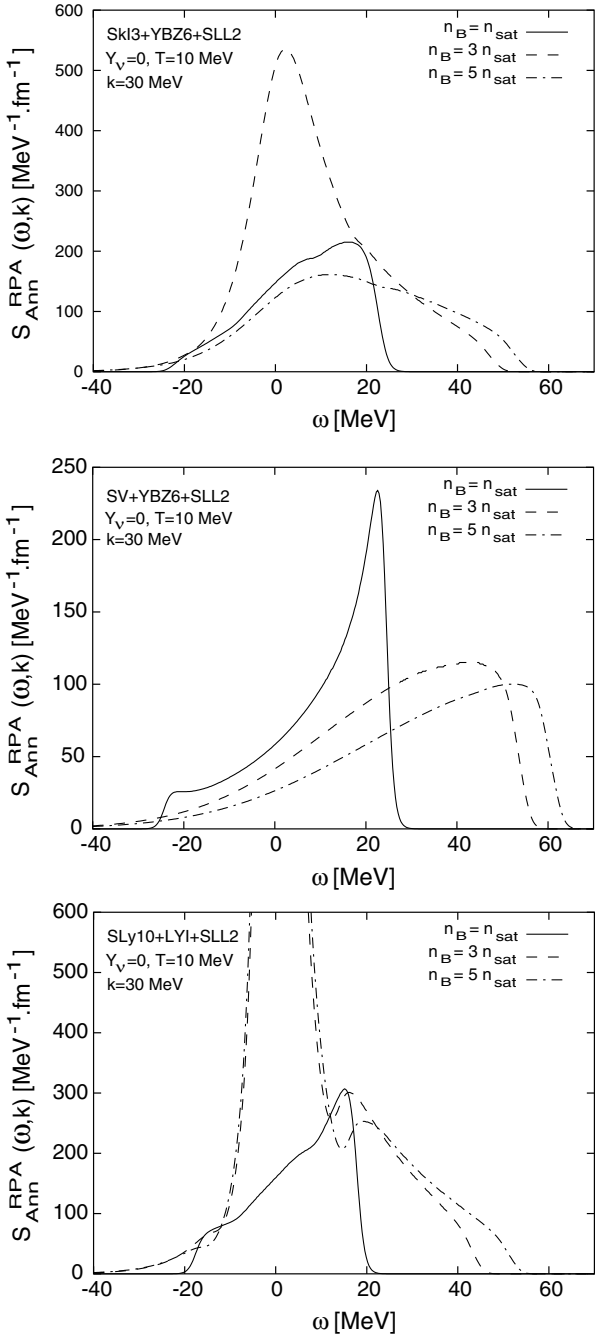

Fig. 5. Axial structure functions in $npe\Lambda$ matter in beta equilibrium in the RPA approximation —comparison of three Skyrme parametrizations.

response is strongly enhanced. The SV+YBZ6+SLL2 parametrization which is free of ferromagnetism accordingly does not give rise to any enhancement at $\omega = 0$.

$S_A^{(pp)}$ follows the usual trend of having its strength shifted to higher ω when density is increased. This is also observed for $S_A^{(nn)}$ in the SV+YBZ6+SLL2 parametrization when the effect is not washed out by the enhancement at $\omega = 0$. At $T = 0$ $S_A^{(\Lambda\Lambda)}$ is only nonzero above the threshold for hyperon production and then qualitatively behaves as $S_A^{(pp)}$. At high density its contribution is of the same order of magnitude as that of the neutrons.

Figure 6 illustrates the temperature dependence of the axial structure functions. In the upper panel, $S_A^{(nn)}$ is represented at $n_B = 4\ n_{\rm sat}$ and $k = 30$ MeV. As the temperature is increased, the response function is enhanced and processes in which the neutrino gain energy in the collision ($\omega < 0$) gradually open. In the lower panel, the hyperon structure function is displayed at $n_B = 2\ n_{\rm sat}$, *i.e.* shortly

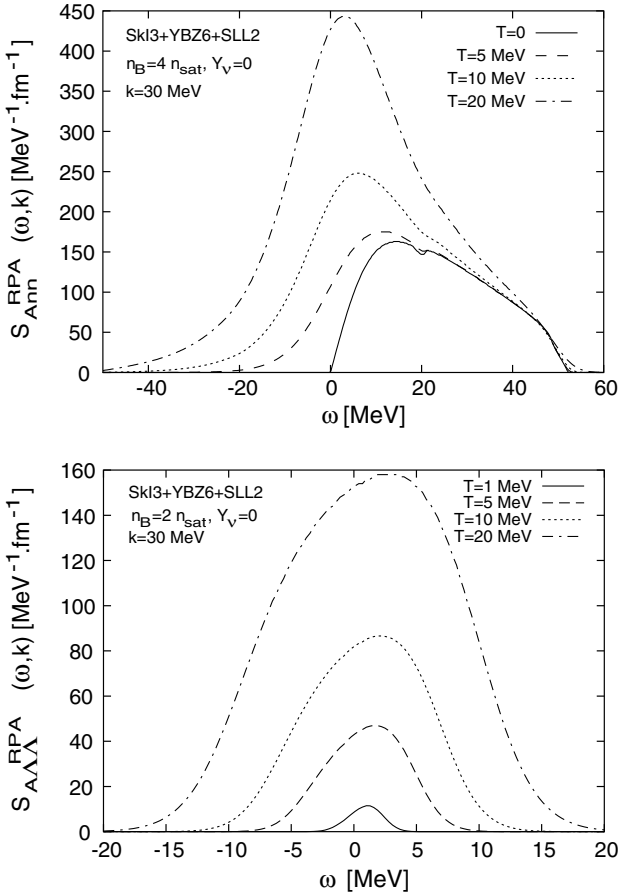

Fig. 6. Axial structure functions in $npe\Lambda$ matter in beta equilibrium in the RPA approximation —temperature dependence.

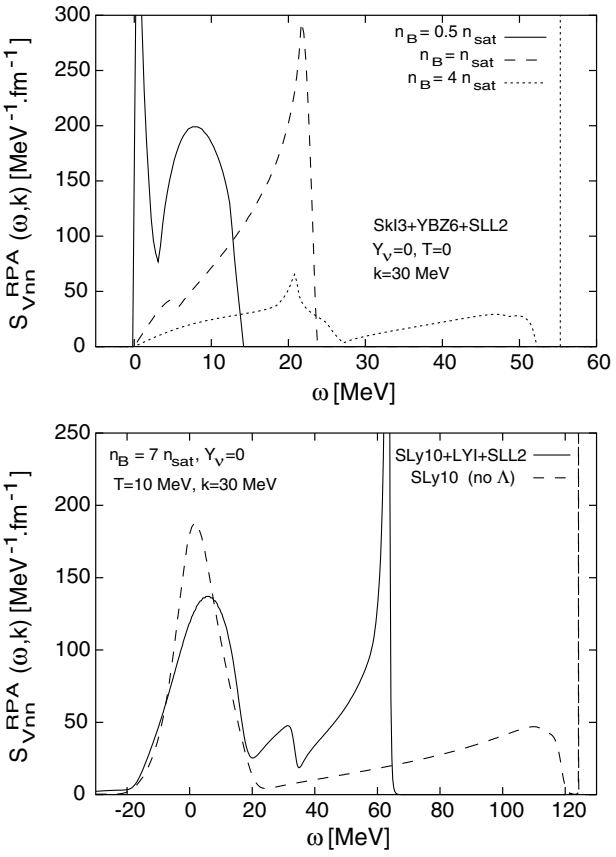

Fig. 7. Vector structure functions in $npe\Lambda$ matter in beta equilibrium in the RPA approximation.

below the threshold density $n^{\Lambda}_{\rm thr} = 2.08\ n_{\rm sat}$. While the structure function vanishes as expected at zero temperature, its contribution increases as temperature rises and rapidly reaches the same order of magnitude as scattering on nucleons: Even though there are only traces of thermally created hyperons in this regime, they contribute actively to the scattering as they are not yet impeded by the Pauli blocking.

b) Vector response

In fig. 7 we show the vector structure function for the neutron. At low density we find when plotting $D_V(\omega, k) = \mathrm{Det}[I - V_{(S=0)}\Pi_0]$ that this function comes near to the zero axis and eventually crosses it. This can be explained as the onset of the spinodal instability, when homogeneous matter is not the stablest state anymore, as is the case at the inner edge of the crust of the neutron star (see, *e.g.*, [36]). As the density is increased, this instability disappears but instead dips form in D_V for a finite value of the energy transfer. When the real part of D_V vanishes a zero sound mode develops. This occurs at approximately 3 $\rho_{\rm sat}$ depending on the equation of state. At moderate densities, the imaginary part is finite and provides for Landau damping of the mode. This is seen on the vector structure function as a peak with some width. At higher density the zero sound mode is unscreened and appears as a delta function outside the vector strength distribution.

We observe that two such dips in D_V develop in npe matter in β equilibrium whereas a third dip appears in $npe\Lambda$ matter. This translates in respectively two or three peaks in the vector response function. The conditions of the lower panel of fig. 7 were chosen so that these features are clearly visible. It is tempting to ascribe each dip to one species of baryons present in the system. As a matter of fact, the position of the dips is approximately given by the characteristic frequencies associated to each particle $\omega_i = k(k + 2p_{Fi})/(2m^*_i)$. The deviation from the exact value is due to the fact that we have mixed states: the isospin is not a good quantum number, neither is the strangeness. For the density range relevant to neutron stars we only see the zero sound associated to the neutrons. The position (*i.e.* velocity) of the zero-sound mode(s) depends on the stiffness of the equation of state. In fig. 7, lower panel, we see that, the equation of state with hyperons being softer than in matter with only neutrons and protons, the zero-sound mode propagates at smaller velocity. The trend is general, and the position of the zero-sound peak for various choices of the NN, $N\Lambda$ and $\Lambda\Lambda$ forces follows their classification according to stiffness realized in [20]: SV+YBZ6 > SkI3+YBZ6 > SLy10+LYI.

Figure 7, upper panel, was drawn at zero temperature. When some temperature is applied to the system (see

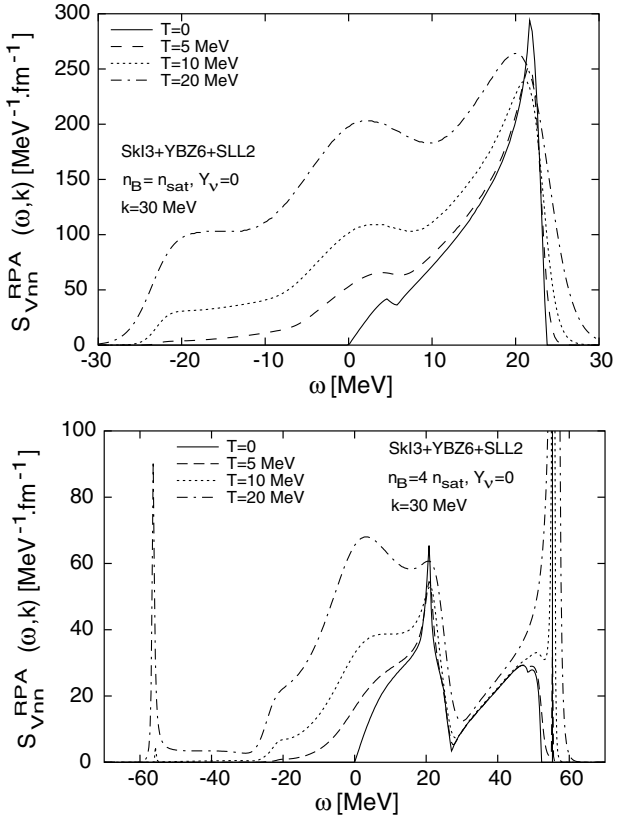

Fig. 8. Vector structure functions in $npe\Lambda$ matter in beta equilibrium in the RPA approximation.

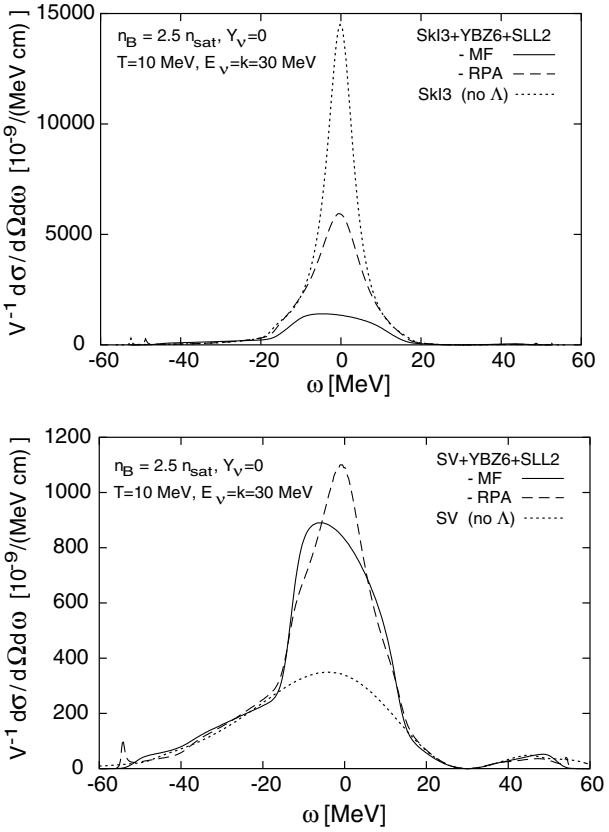

Fig. 9. Differential cross-section in $npe\Lambda$ matter in beta equilibrium in the RPA approximation.

fig. 8), the delta-function (corresponding to an undamped zero-sound mode at $T = 0$) merges with the remaining part of the structure function. As was already observed in the case of the axial response, processes in which the neutrino gain energy in the collision ($\omega < 0$) open as T increases.

c) Differential cross-section

The differential cross-section eq. (4) is displayed on fig. 9 at $n_B = 2.5\ n_{\rm sat}$, *i.e.* shortly above the threshold for hyperon formation. We compare the results for Skyrme models SkI3+YBZ6+SLL2 and SV+YBZ6+SLL2.

Tiny secondary peaks are barely visible at high-energy transfer $\omega = \pm$ 60 MeV. This is what is left of the zero-sound contribution in the vector structure functions (see figs. 7 and 8) after applying the Pauli blocking factor $1 - f(E'_\nu)$. Moreover, in the chosen example $E_\nu = k = 30$ MeV the condition $|\cos\theta| < 1$ restrict the allowed energy ransfer ω to the range $[-k - 2\,E_\nu - k] = [-30\text{–}30]$ MeV, so that the zero sound peak does not contribute altogether.

4.2 Mean free path

The mean free path is obtained by integration of the differential cross-section. This parameter is relevant in the late stages of supernova explosion and first stages of protoneutron star cooling, when the neutrinos are still dynamically trapped in the hot and dense matter.

$$\frac{1}{\lambda} = \sigma = \int \mathrm{d}\omega \mathrm{d}\Omega \left(\frac{\mathrm{d}^2\sigma}{\mathrm{d}\omega \mathrm{d}\Omega}\right)$$
$$= \frac{G_F^2}{4\pi^2} \int_{-\infty}^{E_\nu} \mathrm{d}\omega \frac{E'_\nu}{E_\nu} \int_{|\omega|}^{2E_\nu - \omega} q\mathrm{d}q \left[1 - f(E'_\nu)\right]$$
$$\times \left[(1 - \cos\theta) S_V(\omega, q) + (3 + \cos\theta) S_A(\omega, q)\right]. \tag{26}$$

In the elastic limit where $S_V^{ij} \sim S_A^{ij} \sim S_0^i \delta^{ij} \to 2\pi n_i \delta(\omega)$ for $i, j \in \{n, p, \Lambda\}$ and without Pauli blocking, this reduces to the textbook formula $\frac{1}{\lambda} = \sum_{i=n,p,\Lambda} \frac{1}{\lambda_i} = \sum_{i=n,p,\Lambda} \frac{G_F^2}{\pi} (c_{Vi}^2 + 3c_{Ai}^2)\, E_\nu^2\, n_i$.

We studied the total cross-section and the mean free path for both the neutrino-free and trapped-neutrino case. According to protoneutron star cooling calculations [16], the characteristic energy of the neutrinos is $E_\nu \simeq 3$ T in the former case whereas it is $E_\nu \simeq \mu_\nu$ in the latter case.

Figure 10 shows the mean free path in the mean-field approximation. In the upper panel we have represented the neutrino-free case $Y_\nu = 0$ for a moderate temperature $T = 5$ MeV, while the lower panel displays the case of trapped neutrinos $Y_L = 0.4$ with a higher temperature $T = 20$ MeV. It can be seen that, at the mean-field approximation, the total cross-section is enhanced by

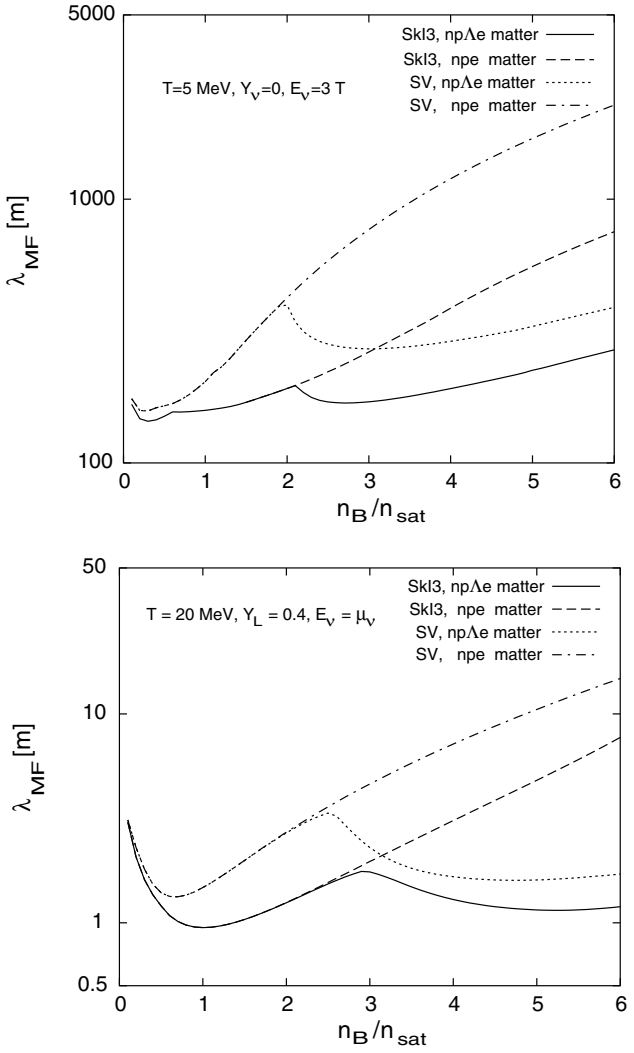

Fig. 10. Mean free path with and without hyperons in the mean-field approximation in neutrino free neutron star matter at $T = 5$ MeV (upper panel), in protoneutron star matter with trapped neutrinos at $T = 20$ MeV, $Y_L = 0.4$ (lower panel).

the apparition of hyperons and the mean free path correspondingly reduced. The same behavior was observed by Reddy *et al.* [6] and explained by the combined effect of the modification of the chemical potentials of the nucleons and the opening of new scattering channels when new degree of freedoms are available. The results of the SkI3+YBZ6+SLL2 and SV+YBZ6+SLL2 are similar, with the mean free path being larger for the SV parametrization corresponding to lower effective masses: At the mean-field level, $\sigma \propto \mathcal{I}\mathrm{m}\Pi_0 \propto m_*^2$ (see eq. (12)) and $\lambda \sim 1/\sigma$.

The mean free path is observed to increase with higher densities. This behavior was also found in nonrelativistic models by Reddy *et al.* [7], whereas relativistic models yield a decreasing mean free path with increasing density. The discrepancy was explained by Reddy *et al.* [7] as the result of two competing mechanisms, *i.e.* the decreasing of the effective masses (see previous *alinea*) and the increase of the chemical potentials: in the nonrelativistic Skyrme model the decreasing m_* is the dominant effect.

The mean free path in the random phase approximation is displayed in fig. 11 in neutrino-free matter in the top panels and with trapped neutrinos in the bottom panels for parametrizations SkI3+YBZ6+SLL2 (left) and SV+YBZ6+SLL2 (right).

We first note an enhancement of the cross-section at subnuclear density for both parametrizations. This is related to the peak present in the vector response function which was noticed in the previous section, and signals the mechanical instability to nonhomogeneous "pasta" phases. Our model is not valid any more in this density range; a calculation would need to be performed along the lines of, *e.g.*, ref. [37].

The dramatic enhancement of the cross-section in the RPA approximation due to the onset of ferromagnetism which was reported in several previous works [7,10,11] is also observed with parameter set SkI3 in *npe* matter. It is indicated in the figure by the line n_{ferro}. The mean free path in *npe* matter goes to zero at this point. When hyperons are present in the system, the ferromagnetic transition can be avoided when the threshold density for hyperon formation is lower than the critical density for ferromagnetism in npe matter [20]. For the set SkI3+YBZ6+SLL2 we have $n^{\Lambda}_{\mathrm{thresh}} = 2.08\ n_{\mathrm{sat}}$, while in npe matter $n_{\mathrm{ferro}} = 3.08\ n_{\mathrm{sat}}$. As a consequence, the pole is avoided and the mean free path goes on gently increasing.

The parameter set SV which was selected as the only Skyrme model in which the ferromagnetic transition does not appear, permits us to study the influence of the RPA corrections in the absence of the pole. We see in the right panels of fig. 11 that the mean free path behaves in this case in a way similar to the mean field result at densities $n_B > n_{\mathrm{sat}}$.

Figure 12 shows the ratio of the total cross-sections $\sigma_{\mathrm{RPA}}/\sigma_{\mathrm{MF}} = \lambda_{\mathrm{MF}}/\lambda_{\mathrm{RPA}}$ in the RPA and mean-field approximation. A residual enhancement in the vicinity of the ferromagnetic instability remaining from the np sector prior to the hyperon formation threshold is visible in the SkI3+YBZ6+SLL2 parametrization. In the SV+YBZ6+SLL2 parametrization the cross-section is somewhat enhanced with respect to the mean-field result: even in the absence of ferromagnetism, this is still at variance with the relativistic prediction [7–9].

We finally explored the impact of the neglect of the other hyperons Σ, Ξ by performing a mean field calculation in the model of Balberg and Gal [21] and another nonrelativistic model based on the Seyler-Blanchard effective interaction by Banik and Bandyopadhyay [38]. Both models include all species of hyperons. The calculation was nevertheless performed here in a reduced version of these models with only the Σ^-- and Λ-hyperons taken into account and no muons. The Σ^--hyperons appear at 1.87 n_{sat} and the Λ at 2.32 n_{sat} in the model of Balberg and Gal with the parameter set corresponding to the choice $\gamma = 4/3$, while the Σ^- are formed at 1.52 n_{sat} and the Λ at 2.82 n_{sat} in the model of Banik and Bandyopadhyay. The mean free path obtained with

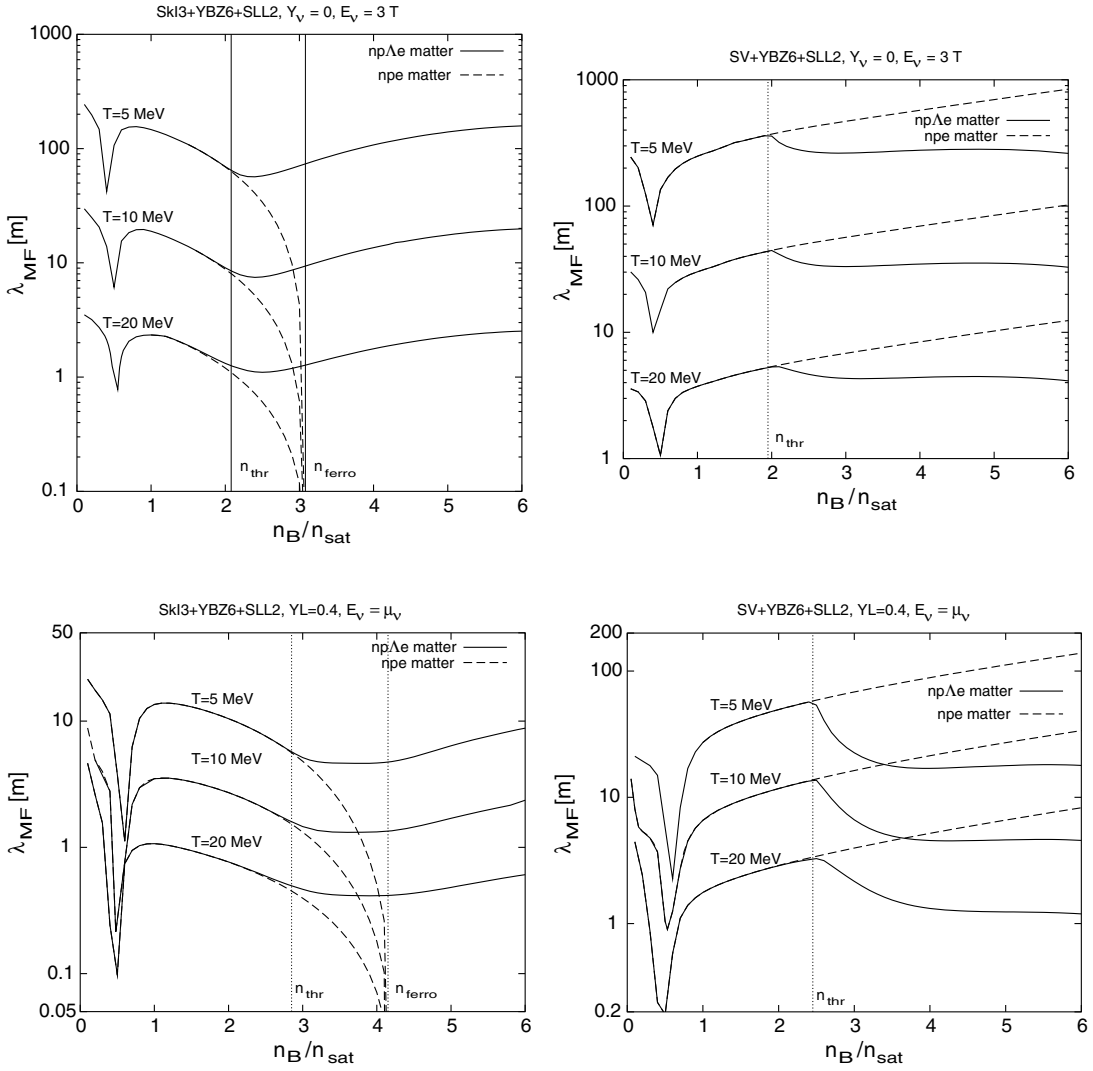

Fig. 11. Mean free path $\lambda_{\rm RPA}$ with and without hyperons in the random phase approximation. On the left-hand side $\lambda_{\rm RPA}$ was calculated with the SkI3+YBZ6+SLL2 parametrization, on the right-hand side with the SV+YBZ6+SLL2 parametrization. Top panels: neutrino-free neutron star matter. Bottom panels: protoneutron star matter with trapped neutrinos ($Y_L = 0.4$).

such models is shown in fig. 13 in neutrino free matter at $T = 10$ MeV for a neutrino of energy $E_\nu = 30$ MeV. The reduction of the mean free path at the formation threshold of a new hyperon is also observed in these models. The effect is less visible for the second hyperon than for the first. The behavior of the mean free path obtained from the model of Banik and Bandyopadhyay is qualitatively similar to that resulting from the Skyrme parametrizations considered in the present work. The decrease of the mean free path with increasing density obtained from the model of Balberg and Gal is easily understood from the fact that whereas both the Skyrme and the Seyler-Blanchard parametrizations have decreasing effective masses, Balberg and Gal keep theirs fixed at the free value (see the discussion below fig. 10).

5 Conclusion

We have performed for the first time a calculation of the neutrino-baryon scattering rates including the hyperons at the RPA level in a nonrelativistic model. The nuclear interactions were described by Skyrme forces calibrated to reproduce the available data on nuclei and hypernuclei and tested for their suitability to describe the properties of neutron stars.

At the mean field level the hyperons open new scattering channels and tend to decrease the mean free path as compared to its value in *npe* matter. In the random phase approximation the cross-section is very sensitive to the degree of stability of the matter with respect to density or spin density fluctuations. The hyperons help delaying or removing the onset of a ferromagnetic instability usually present in Skyrme models. The drastic reduction of the mean free path at the transition is thus avoided. A residual enhancement of the cross-section nevertheless remains in most cases.

Even in the complete absence of a ferromagnetic instability as provided by the parametrization SV+YBZ6+SLL2, we still obtained results which are at

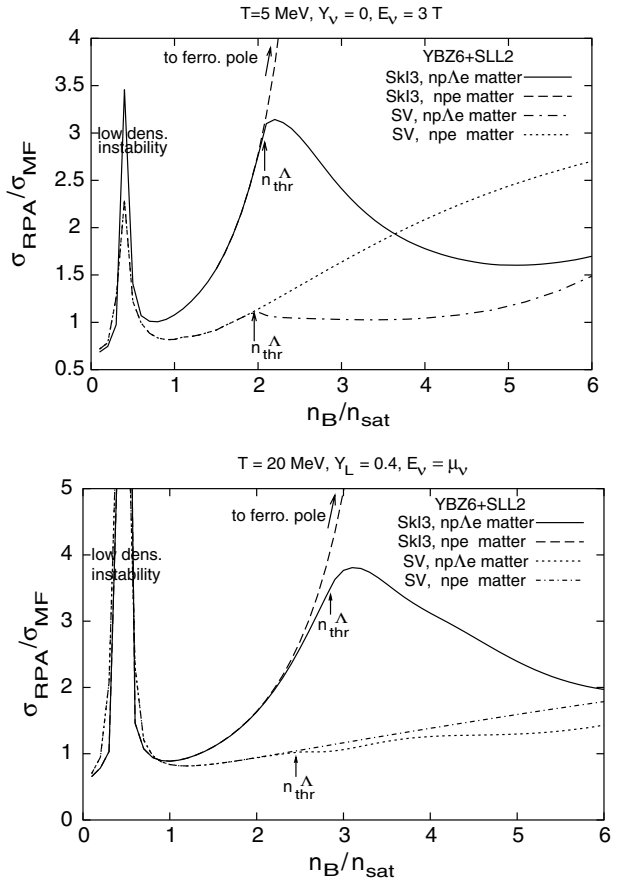

Fig. 12. Enhancement factor for cross-sections calculated in the random phase approximation with respect to mean-field approximation in neutrino free neutron star matter at $T = 5$ MeV (upper panel), in protoneutron star matter with trapped neutrinos at $T = 20$ MeV, $Y_L = 0.4$ (lower panel).

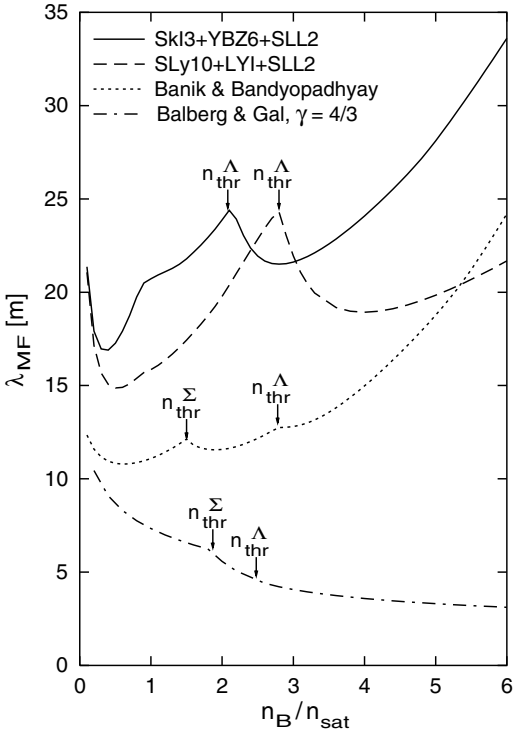

Fig. 13. Mean free path in the mean-field approximation at $T = 10$ MeV, $E_\nu = 3$ T, $Y_\nu = 0$ for various nonrelativistic models of baryonic matter.

variance with the prediction of relativistic models: i) The mean free path increases with density. This may be ascribed to a rapid decrease of the effective masses of the baryons in these models. This feature was observed previously in *npe* matter [7]. ii) The RPA cross-section was still slightly enhanced with respect to the mean field value. This indicates a less repulsive spin interaction as density increases.

Our model is still very schematic. Several items would need to be improved in future work, among which:

i) Particle-hole interaction

The Skyrme interaction was used for convenience in order to keep the model as simple as possible. While it was carefully selected in order to avoid known problems at high density such as the behavior of asymmetry energy, causality and onset of ferromagnetism, it is still being driven at the limit of its reliability. The behavior of the interaction in the spin-spin channel still remains unclear. An other issue is the description of the Λ-Λ force which plays an important role at high density where the hyperon fraction is large, whereas the description of the hyperon-hyperon interaction in phenomenological formalisms is still very poor.

Both points could be substantially improved while still keeping the same level of simplicity for the Dyson equations and neutrino-baryon scattering cross-sections, if we could obtain a parametrization of the polarized energy density functional and effective masses from microscopical variational or Brueckner-Hartree-Fock calculations. Landau parameters extracted from BHF calculations have indeed been used very recently to calculate the neutrino scattering mean free path in neutron matter with the Nijmegen NSC97e potential [12] and for *npe* matter in β equilibrium with the Argonne AV_{18} potential plus 3-body forces [13]. The spin-spin interaction was actually found to be increasingly attractive by both groups, leading to a strongly reduced cross-section in the random phase approximation.

Brueckner-Hartree-Fock calculations also offer a coherent framework to calculate the hyperon-hyperon interaction in medium starting from bare baryon-baryon potentials and then cross checking the results with the data on double hypernuclei. The parametrization of Brueckner results for matter with a hyperonic component is currently under way and will be the subject of another paper [39].

ii) Full RPA

We limited ourselves to the monopolar $l = 0$ Landau approximation. As previous studies in pure neutron matter or symmetric nuclear matter have shown [11,33,34] the full RPA approximation can represent an appreciable correction to the simple $l = 0$ result. While the extension of the full RPA to npΛe matter should not present any conceptual difficulties, the additional amount of work

required is not yet worthwhile, considering the other uncertainties of the model.

iii) Relativistic effects

The main advantage of the nonrelativistic model is that the Dyson equation has a simpler structure, especially if we restrict the calculation to the monopolar approximation. This allows to explore a greater variety of many-body effects and chemical composition of the matter. At the high densities considered in protoneutron stars, a relativistic model however appears to be a desirable requirement.

iv) Charged current processes

The present work explored the role of hyperons in neutrino processes on the example of the scattering through the neutral current. The same methods as used here can be applied to the charged current process. In protoneutron stars, the charged current process $\nu_e + n \rightleftharpoons p + e^-$ is actually dominant. In the subsequent long cooling phase, the triangle rule for conservation of momentum constrained to the immediate vicinity of the Fermi surface is less restrictive in the direct URCA process involving hyperons such as $p + e^- \rightleftharpoons \Lambda + \nu_e$, which makes this an interesting mechanism for an efficient cooling of the star [40].

This work was supported by the Spanish-European (FICYT/FEDER) grant number PB02-076. Part of it was realized during a stay at the Departament d'Estructura i Constituents de la Materia of Barcelona University. Several discussions with A. Polls are gratefully acknowlegded.

References

1. M. Liebendörfer, M. Rampp, H.-Th. Janka, A. Mezzacappa, astro-ph/0310662; M. Liebendörfer, A. Mezzacappa, F.K. Thielemann, O.E.B. Messer, W.R. Hix, S.W. Bruenn, Phys. Rev. D **63**, 103004 (2001); T.A. Thompson, A. Burrows, P.A. Pinto, Astrophys. J. **592**, 434 (2003).
2. N. Iwamoto, C.J. Pethick, Phys. Rev. D **25**, 313 (1982).
3. C.J. Horowitz, K. Wehrberger, Nucl. Phys. A **531**, 665 (1991).
4. A. Burrows, R.F. Sawyer, Phys. Rev. D **58**, 554 (1998).
5. A. Burrows, S. Reddy, T.A. Thompson, astro-ph/0404432.
6. S. Reddy, M. Prakash, J.M. Lattimer, Phys. Rev. D **58**, 013009 (1998).
7. S. Reddy, M. Prakash, J.M. Lattimer, J.A. Pons, Phys. Rev. C **59**, 2888 (1999).
8. S. Yamada, H. Toki, Phys. Rev. C **61**, 015803 (1999).
9. L. Mornas, A. Pérez, Eur. Phys. J. A **13**, 383 (2002).
10. J. Navarro, E.S. Hernandez, D. Vautherin, Phys. Rev. C **60**, 045801 (1999).
11. J. Margueron, PhD Thesis, Orsay University, France (2001).
12. J. Margueron, I. Vidaña, I. Bombaci, Phys. Rev. C **68**, 055806 (2003).
13. W. Zuo, Caiwan Shen, N. Van Giai, Phys. Rev. C **67**, 037301 (2003); Caiwan Shen, U. Lombardo, N. Van Giai, W. Zuo, Phys. Rev. C **68**, 055802 (2003).
14. P. Bernardos, S. Marcos, R. Niembro, M.L. Quelle, Phys. Lett. B **356**, 175 (1995).
15. T. Maruyama, T. Tatsumi, Nucl. Phys. A **693**, 710 (2001).
16. J.A. Pons, S. Reddy, M. Prakash, J.M. Lattimer, J.A. Miralles, Astrophys. J. **513**, 780 (1999).
17. D.E. Lanskoy, Y. Yamamoto, Phys. Rev. C **55**, 2330 (1997).
18. D.E. Lanskoy, Phys. Rev. C **58**, 3351 (1998).
19. Y. Yamamoto, H. Bandō, J. Žofka, Prog. Theor. Phys. **80**, 757 (1988).
20. L. Mornas, *Neutron stars in a Skyrme model with hyperons*, submitted to Eur. Phys. J. A.
21. A. Balberg, A. Gal, Nucl. Phys. A **625**, 435 (1997).
22. J. Mares, E. Friedman, A. Gal, B.K. Jennings, Nucl. Phys. A **594**, 311 (1995).
23. C.J. Batty, E. Friedman, A. Gal, Phys. Rep. **287**, 385 (1997).
24. J. Dabrowski, Phys. Rev. C **60**, 025205 (1999); Acta Phys. Pol. B **35**, 971 (2004).
25. K. Tsushima, K. Saito, J. Haidenbauer, A.W. Thomas Nucl. Phys. A **630**, 691 (1998).
26. M. Kohno, Y. Fujiwara, T. Fujita, C. Nakamoto, Y. Suzuki, Nucl. Phys. A **674**, 229 (2000).
27. J. Schaffner-Bielich, A. Gal, Phys. Rev. C **62**, 034311 (2000).
28. P.G. Reinhard, H. Flocard, Nucl. Phys. A **584**, 467 (1995).
29. E. Chabanat, P. Bonche, P. Haensel, J. Meyer, R. Schaeffer, Nucl. Phys. A **635**, 231 (1998).
30. M. Beiner, H. Flocard, N. Van Giai, P. Quentin, Nucl. Phys. A **238**, 29 (1975).
31. M. Prakash, I. Bombaci, M. Prakash, P.J. Ellis, J.M. Lattimer, R. Knorren, Phys. Rep. **280**, 1 (1997).
32. C. García Recio, J. Navarro, N. Van Giai, L.L. Salcedo, Ann. Phys. (N.Y.) **214**, 293 (1992).
33. E.S. Hernández, J. Navarro, A. Polls, Nucl. Phys. A **627**, 460 (1997); **658**, 327 (1999).
34. F.L. Braghin, D. Vautherin, A. Abada, Phys. Rev. **52**, 2504 (1995).
35. V. Baran, M. Colonna, M. Di Toro, A. Larionov, Nucl. Phys. A **632**, 287 (1998); V. Baran, M. Colonna, M. Di Toro, V. Greco, Phys. Rev. Lett. **86**, 4492 (2001).
36. C.P. Lorenz, D.G. Ravenhall, C.J. Pethick, Phys. Rev. Lett. **70**, 379 (1993); F. Douchin, P. Haensel, Phys. Lett. B **485**, 107 (2000).
37. C.J. Horowitz, M.A. Pérez-García, J. Piekarewicz, Phys. Rev. C **69**, 045804 (2004).
38. S. Banik, D. Bandyopadhyay, J. Phys. G **26**, 1495 (2000).
39. I. Vidaña, A. Rios, L. Mornas, A. Polls, A. Ramos, *Parametrization of Brueckner-Hartree-Fock calculations for polarized baryonic matter*, in preparation.
40. D.G. Yakovlev, A.D. Kaminker, O.Y. Gnedin, P. Haensel, Phys. Rep. **354**, 1 (2001).